

# Time-frequency analysis via deconvolution with sparsity constraints

David Bonar\*

Department of Physics, University of Alberta, Edmonton, Alberta, Canada  
bonar@ualberta.ca

and

Mauricio D. Sacchi

Department of Physics, University of Alberta, Edmonton, Alberta, Canada

Hong Cao

Research Institute of Petroleum Exploration & Development, PetroChina, China

Xin-Gong Li

Shell International E&P Inc and Integration Seismic Solution Inc, USA

## Summary

Spectral decomposition is a time-frequency analysis tool widely used for seismic data interpretation. Compared to conventional frequency analysis, spectral decomposition attempts to estimate the frequency content of the seismic signal at any particular time. This type of analysis has commonly been achieved using, for instance, the short window Fourier transform to determine the localized frequency content of the seismic signal. An alternative method is proposed in which the seismic signal is deconvolved with a dictionary of different central frequency Ricker wavelets. This approach allows for different frequency components of the seismic signal to be accounted for with different Ricker wavelets. By applying sparsity constraints, greater resolution is obtained in the time-frequency distribution since a minimal number of Ricker wavelets are required to fit the original seismic signal.

## Introduction

The frequency content of a given time series (i.e. a seismic signal) is commonly found using the Fourier transform. However, the frequency information obtained from this procedure relates to the entire time series and contains no information about local frequency variations. Time-frequency analysis, also known as spectral decomposition, attempts to obtain the local frequency content of the time series rather than the global frequency content that is obtained from the Fourier transform. The local frequency map obtained via spectral decomposition has been employed in reservoir characterization to study thin beds (Partyka et al., 1999) and the low frequency shadows associated with hydrocarbons (Castagna et al., 2003).

Time-frequency analysis has commonly been performed using short window discrete Fourier transforms (Partyka et al, 1999). In this type of time-frequency analysis, the reflectivity sequence, which represents the geological sequence, can no longer be considered white, or completely random. Therefore, the spectral attributes seen in the amplitude spectrum of the short-window Fourier transform are a combination of the amplitude spectrums of the seismic wavelet and reflectivity sequence. It is this interference attribute of the wavelet and reflectivity amplitude spectra that has been exploited in earlier time-frequency analysis exercises. Various other approaches have also been developed for time-frequency analysis such as the continuous wavelet transform (Sinha et al., 2005), S-transform (Stockwell et al., 1996), and matching pursuit algorithms (Mallat and Zhang, 1993).

This article proposes an alternative time-frequency analysis technique for seismic signals. We utilize a high-resolution sparsity promoting approach to retrieve a set of frequency dependent reflectivity series. The frequency content of the seismic signal at a given time is obtained from the set of Ricker wavelets that characterize that particular portion of the seismic signal.

Applying sparsity constraints to the deconvolution procedure enhances resolution of the time-frequency analysis.

## Theory

The convolutional model states that a seismic trace,  $s$ , is composed of the convolution of a wavelet,  $w$ , with the reflectivity sequence,  $r$ , of the Earth as seen in Equation 1. This equation

$$s = w * r \quad (1)$$

can also be represented as the linear system of equations,  $s = Wr$ , where  $W$  represents the convolutional matrix of the wavelet. Instead of viewing how one individual wavelet is represented in the seismic trace, we will study how multiple wavelets can be represented in the seismic trace. Using a dictionary of different Ricker wavelets, which are uniquely defined by a central frequency (Ryan, 1994), the seismic trace can be decomposed into its different frequency components at a specific time through the employment of deconvolution. If  $N$  different frequency Ricker wavelets comprise the Ricker wavelet dictionary, the seismic trace can be constructed from its frequency components by

$$s = \begin{pmatrix} W_1 & W_2 & \dots & W_N \end{pmatrix} \begin{pmatrix} r_1 \\ r_2 \\ \vdots \\ r_N \end{pmatrix} = Dm \quad (2)$$

where  $W_i$  and  $r_i$  refer to the wavelet convolution matrix for the Ricker wavelet with central frequency  $f_i$ , and its associated reflectivity sequence. The matrix  $D$  represents the dictionary of Ricker wavelets and, finally,  $m$  is used to represent the vector containing all the pseudo-reflectivity sequences. Essentially, the seismic signal is decomposed into several traces that are uniquely determined from a singular Ricker wavelet and its related reflectivity structure. The time-frequency analysis can then be obtained with the prior knowledge of the frequency content of the individual Ricker wavelets. Thus, the seismic signal can be transformed into a time-frequency map by deconvolving a Ricker wavelet dictionary from the seismic signal to obtain a pseudo-frequency dependent reflectivity structure that can be portrayed as a time-frequency map.

To increase resolution in the time-frequency map, sparsity constraints are applied during the deconvolution process. By imposing that the solution, or pseudo-frequency reflectivity structure, be sparse, a minimal amount of Ricker wavelets will be required to represent the seismic signal. This in turn will make the pseudo-frequency reflectivity structure and thus, the time-frequency map have a greater resolution. The sparsity constraints are imposed by considering a mixed  $l_2 - l_1$  norm problem, as the  $l_1$  regularization term constrains the solution to be sparse. The resulting cost function to be minimized is given by

$$J = \|s - Dm\|_2^2 + \lambda \|m\|_1 \quad (3)$$

where  $\lambda$  is the regularization parameter that controls the amount of sparseness desired in the solution.

The mixed  $l_2 - l_1$  norm problem was solved using two different techniques, IRLS (Daubechies, 2009) and FISTA (Beck and Teboulle, 2009). The iteratively reweighted least squares method, or IRLS, solves the cost function in a similar way that the regularized least squares method solves the  $l_2 - l_2$  norm problem and is described by Equation 4 where the matrix  $Q$  implicitly

$$m_{k+1} = (D^T D + \lambda Q)^{-1} D^T s \quad (4)$$

depends upon the original model  $m_k$ . The conjugate gradient method was employed to make this algorithm more efficient. The fast iterative shrinkage-thresholding algorithm, or FISTA, is based upon the idea of iteratively solving simpler cost functions that are always greater than the original, complex cost function using a soft-thresholding operator. This method can be described using Equation 5 where  $\alpha$  is a constant that must be greater than or equal to the

$$m_{k+1} = \text{soft}\left(h_k + \frac{1}{\alpha} D^T \left(s - Dh_k\right), \frac{\lambda}{2\alpha}\right) \quad (5)$$

maximum eigen value of  $D^T D$  and  $h_k$  is a clever update of the model estimate  $m_k$ .

## Examples

A synthetic seismogram was created with a 15 Hz Ricker wavelet at 0.1s, a 30 Hz Ricker wavelet at 0.2s, a 45 Hz Ricker wavelet at 0.3s, 60 Hz and 45 Hz Ricker wavelets around 0.4s, and 15 Hz, 45 Hz and 60 Hz Ricker wavelets around 0.5s. This synthetic seismogram and the time-frequency analysis obtained from the non-sparse regularized least squares solution, the IRLS solution, and the FISTA solution are displayed in Figure 1. As can be seen, by imposing sparsity constraints during the deconvolution procedure increased resolution in the time-frequency map was achieved. This increased resolution made it more apparent that there were separate events that were located around 0.4s and 0.5s. The results obtained from the IRLS and FISTA methods are also comparable to one another for roughly equal run times. The synthetic seismogram created for Figure 1 was also contaminated with 5% noise and the resulting time-frequency analysis is depicted in Figure 2. The results of this exercise are still quite similar to the non-noisy case.

We have applied the proposed method to 3D seismic data from central China. Figures 3 and 4 show a seismic amplitude cross-section and its high-resolution spectral decomposition from this data set. Only the positive amplitudes are displayed for the high-resolution spectral decomposition, which is shown in an RGB display of three identified frequency bands. The red arrow in these figures represents the base of a sand zone and is displayed as a time slice of the amplitude and high-resolution spectral decomposition volumes in Figures 5 and 6, respectively. Based on the limited well information, gas existence is correlated more with low frequency signatures rather than seismic amplitudes. There could be several reasons that the gas production relates to a low frequency signature (Castagna et al., 2003) such as the gas, under in situ conditions, has decreased the seismic velocity, which increases the time-thickness of the zone of interest. Tuning effects on the seismic signal would thus change, causing the lower frequency signature.

## Conclusion

An alternative method for time-frequency analysis was proposed by deconvolving a Ricker wavelet dictionary from a seismic signal. By imposing sparsity constraints, the proposed time-frequency analysis method produced a higher resolution image. Due to the more complicated nature of solving the deconvolution problem with sparsity constraints, two sparse solving methods, IRLS and FISTA, were suggested and produced similar results. Testing on a field data set showed the high resolution spectral decomposition provides a good correlation between the low frequency amplitude and gas production.

## Acknowledgements

We would like to thank NSERC for supplying the funding for this research as well as the members of SAIG (Signal Analysis and Imaging Group) for their support

## References

Beck, A., and Teboulle, M., 2009, A fast iterative shrinkage-thresholding algorithm for linear inverse problems: SIAM J. Imaging Sciences, 2, 183-202.

Castagna, J. P., Sun, S. J., and Siegfried, R. W., 2003, Instantaneous spectral analysis: Detection of low-frequency shadows associated with hydrocarbons: *The Leading Edge*, 22, 120-127.

Daubechies, I., Devore, R., Fronasier, M., and Gunturk, S., 2009, Iteratively re-weighted least squares minimization for sparse recovery: *Commun. Pure Appl. Math.*

Mallat, S. G., and Zhang Z., 1993, Matching pursuits with time-frequency dictionaries: *IEEE Transactions on Signal Processing*, 41, 3397-3415

Partyka, G., Gridley, J., and Lopez, J., 1999, Interpretational applications of spectral decomposition in reservoir characterization: *The Leading Edge*, 18, 353-360.

Ryan, H., 1994, Ricker, Ormsby, Klauder, Butterworth – A choice of wavelets: *CSEG Recorder*, 7, 8-9.

Sinha, S., Routh, P. S., Anno, P. D., and Castagna, J. P., 2005, Spectral decomposition of seismic data with continuous-wavelet transform: *Geophysics*, 70, P19-P25.

Stockwell, R. G., Mansinha, L., and Lowe, R. P., 1996, Localization of the complex spectrum: the S transform: *IEEE Transactions on Signal Processing*, 44, 998-1001.

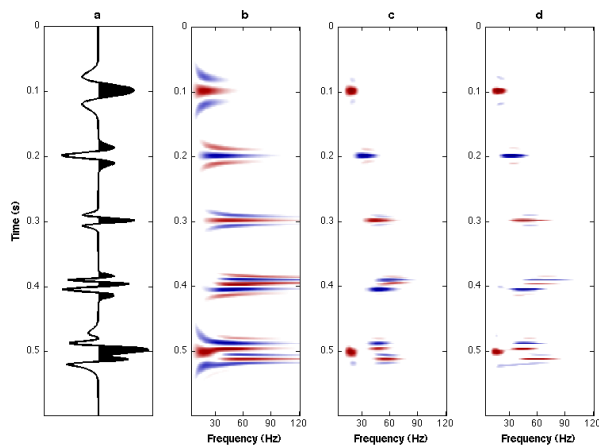


Figure 1: Synthetic example without noise; (a) synthetic seismic signal; (b) non-sparse solution; (c) IRLS solution; (d) FISTA solution

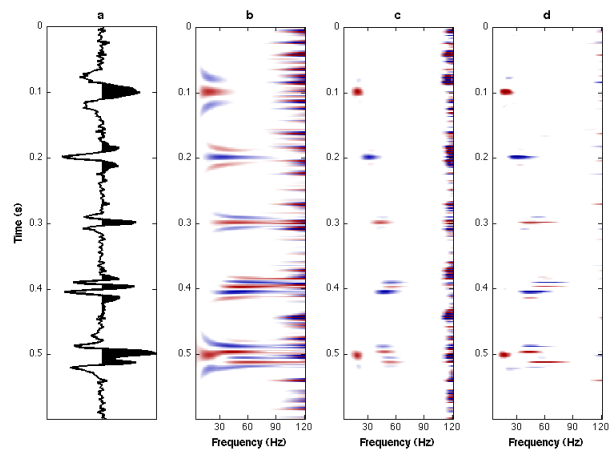


Figure 2: Synthetic example with noise; (a) synthetic seismic signal; (b) non-sparse solution; (c) IRLS solution; (d) FISTA solution

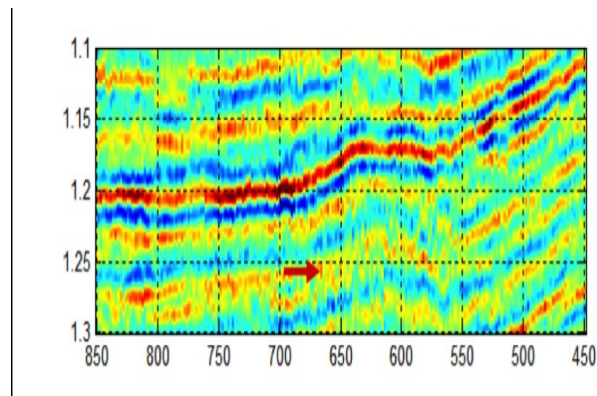


Figure 3: Seismic amplitude cross-section for central China data. Red arrow corresponds to the base of a sand zone at a producing well near line 670.

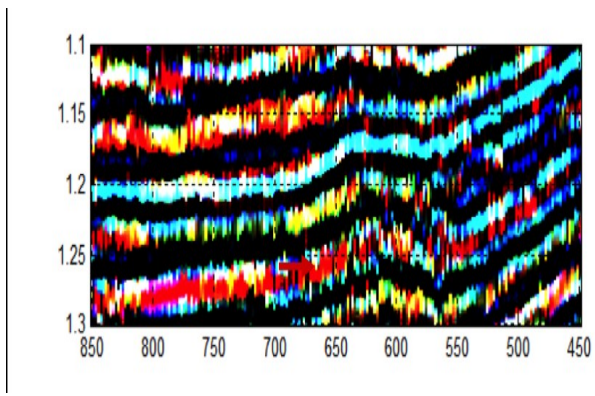


Figure 4: RGB display of the high-resolution spectral decomposition of Figure 3 with red/green/blue showing the frequency bands 10-21, 22-28 and 28-40 Hz, respectively.

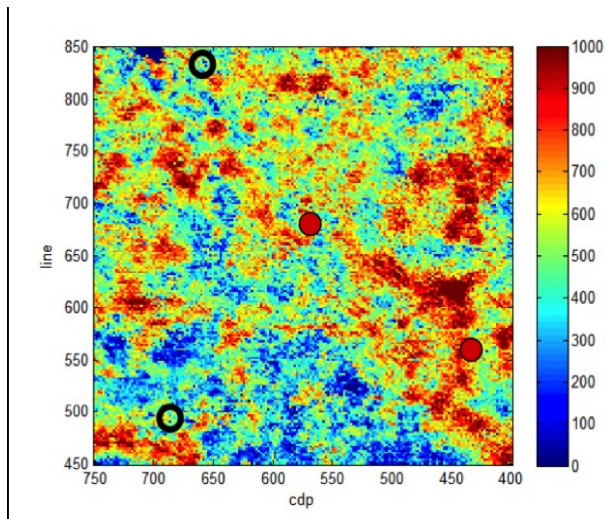


Figure 5: Amplitude time slice at base of sand zone shown in Figure 3. There are four wells in the area, two dry (open circles) and two gas (red filled circles).

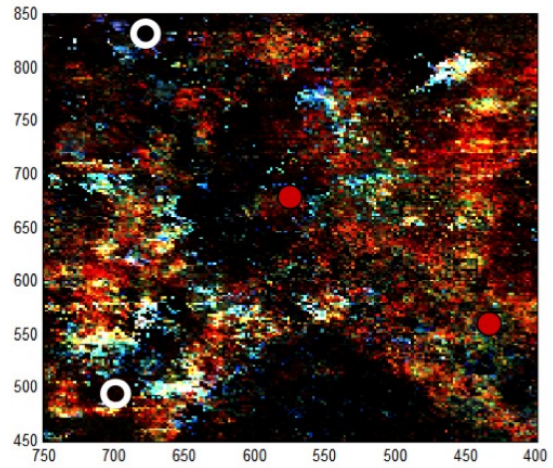


Figure 6: Time slice of high-resolution spectral decomposition at the zone of interest. The production correlates quite well with low frequency signatures (red) as opposed to the seismic amplitudes of Figure 5.